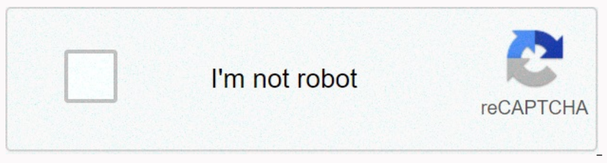

Continue

Amyloid beta fibril formation

Alzheimer's disease (AD) pathology is characterized by plaques of amyloid beta (Aβ) and neurofibrillary sangles tau. Aβ aggregation is thought to take place in the early stages of the disease and eventually give way to the formation of tau tangles that monitor human cognitive decline. Here we understand the crystal structure of the Aβ core segment determined by MicroED and this, note the properties of both fibrillar and oligomeral structure. Using this structure, we designed peptide-based inhibitors that reduce Aβ aggregation and toxicity of species that have already been aggregated. Unexpectedly, we also found that these inhibitors reduce the effectiveness of Aβ-mediated tau aggregation and also reduce the addition and self-seeding of tau fibrils. The ability of these inhibitors to interfere with both Aβ and tau seeds shows that these fibrils share a common epitope, and supports the hypothesis that cross-seeding is one mechanism by which amyloid is associated with tau aggregation and may promote cognitive decline. Alzheimer's disease (AD) is the most common form of dementia, there is limited treatment for symptom relief and none that stops its progression. Histological properties of AD are extracellular patches of amyloid beta (Aβ) and intracellular neurofibrilary sangles tau (Glenner et al., 1984; (2017) (2017) Although Aβ aggregation is thought to occur in the early stages of AD, tau aggregation correlates better with disease progression, characteristic spreads along related brain regions, and the severity of symptoms observed in the wearing (Tanzi, 2012; Hardy and Selkoe, 2002; Manczak and Reddy, 2014; Seward et al., 2013; Brier et al., 2016; Schwarz et al., 2016). Structural information on aggregated forms of Aβ and tau accumulates, but to date this knowledge has not led to successful chemical intervention (Chen et al., 2017). In transgenic mouse models that have occurred by overcoming or co-expressing mutantaβ and mutanttau, a link between the appearance of Aβ and tau pathologies has been observed, but the mechanism has not yet been understood at the molecular level (Oddo et al., 2003). By injecting Aβ seeds derived from a synthetic peptide, transgenic mouse or AD patient tissue, tau pathology can be found both at the injection site, and also in functionally connected brain regions (Bolmont et al., 2007; Götz et al., 2001; Morales et al., 2015). Tau aggregation is also monitored by Aβ-seeded 3D neurons in stem cell cultures that express early onset hereditary mutations that drive overproduction and aggregation of Aβ (Choi et al., 2014). Despite these observations, Aβ's molecular link to Tau remains unresolved. The proposed hypotheses include Aβ causing next stage cell changes that cause tau phosphorylation and final aggregation, and/or direct tau interaction and sowing of aggregated Aβ (Ittner and Götz, 2011; Stancu et al., 2014; Morales 2013. A number of evidence supports the direct interaction model, although questions remain; for example, how such interaction may occur because Aβ spots deposit outside the cell, while tau neurofibrilary tangle is intracellular. One possible model for intracellular aggregation may be that Aβ is rendered in app inside the endosomes, and then exported (Rajendran et al., 2006). The second model proposes that smaller differential Aβ oligomers are toxic species (Lesné et al., 2006; Lambert et al., 1998; Benilova et al., 2012); Oligomers separated from Aβ serum are sufficient to induce tau aggregation (Jin et al., 2011). Aβ is also found in combination with localization intra-neuronally with tau as well as synaptic terminals, increased interactions correlated with disease progression (Manczak and Reddy, 2014). In addition, there are AD tissue extracts (Manczak and Reddy, 2014; Guo et al., 2006). Aβ and Tau soluble complexes have been found in vitro to promote tau (Guo et al., 2006), while another study found that Aβ fibrils may be sown with tau (Vasconcelos et al., 2016). The evidence of taking together hypotheses that Tau cross-seeding by Aβ promotes the tangle formation of AD, which can be prevented not only by inhibiting Aβ aggregation, but also by disrupting the binding area of Aβ with tau. A number of interactions have been offered for both proteins. In Aβ, both the amyloid core klvffa and the areas supporting the residues of the carboxy terminal were found to bind to tau (Guo et al., 2006). On the other hand, it was found that peptides from tau regions exons 7 and 9, as well as aggregation-prone sequences VQIINK and VQIVYK, located at the beginning of repetition 2 (R2) and repeated 3 (R3) microtubules in the domain (K18), were found to bind Aβ (Guo et al., 2006). The calculated seedling model predicts that the amyloid core of Aβ may form intermolecular β-leaf interactions with VQIINK or VQIVYK (Miller et al., 2011). On this basis, we assumption that an inhibitor capable of attacking the amyloid nucleus, which itself is an important jar of Aβ aggregation (Tjernberg et al., 1999; Bernstein et al., 2005; Marshall et al., 2016), may block both Aβ aggregation and tau seeding with Aβ. However, this segment has been observed in several body structures stericzipper structures (Colletier et al., 2011) and fiber models (Lührs et al., 2005; Colvin et al., 2016; Qiang et al., 2012; Huber et al., 2015; Wälti et al., 2016), obstructing the design of a structural inhibitor. In an effort to characterize this complex of toxic body building, we focused our efforts on determining the structure of segment 16-26, which included iowa's early hereditary mutation D23N (Van Nostrand et al., 2001). Based on this structure, we designed several inhibitors and found that they did indeed block Aβ aggregation, prevented Tau from cross-seeding by Aβ and surprisingly also blocked homotheneous. We recommend that the effectiveness of these structural inhibitors for both proteins, but not other amyloidfibrils, suggests there is a similar binding interface displayed in both Aβ and tau aggregates, supporting the cross-amyloid cascade hypothesis ad. With crystals that are only a few hundred nanometers thick, we used microElectron fraction (MicroED) to determine the structure of Aβ residues 16-26 containing hereditary mutation D23N (Figure 1A), KLVFFAENVGS. The structure showed a pair of anti-parallel β-leaves each consisting of ~4,000 strands, stacked in a fibril that extends across the length of the crystal. The adjacent leaves are oriented back to face (Figure 1B, Table 1), which define the class seven with a steric zipper motif. A) The electron micrograph of 3D crystals used for data collection shall be 1 µm. (B) The structure of the crystal shows a pair of β of closely mating antiparalling and semi-detached leaves with magnetic leaves in grey and cyan. Side circuits intertwine to form a dry interface. The two neighbouring pages are β with the leaves. C) View of six layers perpendicular to the fibriil axis (black line). β-pages stack check out along the fibril axis. KLVFFAENVGSExcitation Voltage (kV)200Electron Sourcefield emission gunWave length (Å)0.0251 Total dose per crystal (e-/ Å2)2.7Ram speed (frame/s)0,3 to 0,5Speed (°/s)0,3 crystals used13 Total angle rotation collected (°)941 Combining StatisticsSpace groupP21Cell dimensionsa, b, (c)11.67, 51,91, 12,76α, β, γ (°)90, 114.18, 90Sa 11.64-1.4 (1.44-1.40)*Rmerge24.0% (65.2%)No. Reflections47 598 (1966)Unique Reflections2355 (163)Completeness (%)86.2% (78.0%)Throwiness21 (12)I/σ9.06 (2.88)CC1/299.5% (69.7 %)Refining Statistics No. reflections2354 Reflections in test kit236Rwork23.7%Rfree28.3%R.m.s. deviationsBond lengths (Å)0.014Bond angles (°)1.5Avg. B factor (Å2)9.46Wilson B factor (Å2)7.2Ramachandran (%)Favored100%Allowed0%Outliers0 In addition, three residues from terminal C are adopted by an extended, β body structure which stabilises the packaging between stericzippers (Figure 1 – Figure 1). The sheet interface is reinforced by interfering side chains, Lys 16, Val18, Phe20, Glu22 from one branch face and Leu17, Phe19 and N-terminus from the other. Zipper has an extensive interface with high-shaped complementarity of 0.76 and the total buried solvent accessible area 258 Å2. This structure is partly identical to the structure of the shorter peptide segment Aβ16-21, KLVFFA (crystalform-I) (Colletier et al., 2011), which we successfully used as a search model for molecular replacement. Both longer and shorter segments have seventh-class symmetry. However, the two segments differ from the registry. As a shorter segment, the property has a hydrogen binding pattern, while the longer segment is unregistered. It is that tilted perpendicular to the fibile axis – a deviation from β architecture. This elongated beta chain of residues 16-22 has also been observed in the total length of fibrill oil determined by cryome (Figure 1 – Figure 2) (Gremer et al., 2017). The anti-parallallal architecture and absence of a 16-26 registration indicate that this crystalline fibrillary-like combination has some amyloidoligomer properties. Structural studies of amyloid oligomers most commonly reveal anti-parallel β of page architecture (Tay et al., 2013; Laganowsky et al., 2012; Sarkar et al., 2014), while fibile structures have shown parallel β (Lührs et al., 2005; Colvin et al., 2016; July 2016. Krotee et al., 2018), with the exception of a few short segments of Aβ (Colletier et al., 2011) and Aβ1-40, which contain early onset hereditary mutation D23N, which leads to unregistered anti-parallel fiber contamination spots (Qiang et al., 2012; Tycko et al., 2009). Anti-endik-β of branches outside the register have been proposed to be toxic oligomers (Laganowsky et al., 2012; Liu et al., 2012). In segment Aβ16-22, it is proposed to form such oligomers in silica (Sun et al., 2018). Aβ16-21, Aβ16-26 and full-length fibrill structures may provide clues to the design of inhibitors that prevent both fibrillar and oligomers from being identified. Since the zipper motif observed in the atomic structure of Aβ16-26 D23N may be relevant for different amyloid beta nodes, we tried to use it to develop Aβ1-42 structural-based peptide inhibitors. Our laboratory has developed a Rosetta-based design strategy using steric zipper structures to design capping peptide inhibitors for a number of amyloid proteins associated with the disease (Sievers et al., 2011; Seidler et al., 2018; Saelices et al., 2015; Soragni et al., 2016; krotee et al., 2018). We chose to cut back on our structure scrap from 16 to 22 search model, leaving the residue not β course of action. We threaded amino acids onto capping β direction and minimized energy communication circuits. From our first design round, we selected six different inhibitor candidates; those identified as good candidates but contained strong amino acid similarities to other top inhibitors were eliminated. Our initial group of inhibitors contained four L-form peptides, 2 for every 6 and 8 amino acids in length, called L1-L4, and two D-peptides with six amino acids long, called D1 and D2. We evaluated the effectiveness of inhibitors with 10 mole surpluses by testing whether they prevented Aβ1-42 toxicity to Neuro-2a (N2a) cells, mouse neuroblastoma cell line (Olmsted et al., 1970). We measured cytotoxicity using 3-(4,5-dimethylthiazole-2-yl)−2,5-diphenyltetrazolium bromide (MTT) dye reduction (Mosmann, 1983; Liu et al., 1997). Our toxicity analysis showed a single inhibitor, D1 jada (D)-LYIWVQ, which was able to eliminate toxic effects Aβ1-42 additional dossier 1); none of the inhibitors was toxic to N2a cells only (Figure 2 – Figure 1A). In the inhibitor molecular model, the smaller hydrophobic residues of D1 mimic the interactions with the fible interface on one side of the peptide, which promotes recognition (Figure 2B), while the other half of the peptide places large aromatic residues between aβ residues, blocking possible further interactions (Figure 2C). A) Identification of the Aβ1-42 inhibitor. 10 µM Aβ1–42 was incubated alone or 100 µM with each candidate peptide inhibitor for 12 hours at 37 °C and then diluted at 1:10 with pre-plated N2a cells. Cytotoxicity was quantified by MTT colour reduction bars, which are average for individual replicates, with one standard deviation (n = 3; ns = not significant; ****, p<0,0001 using the usual one-way ANOVA-Dunnett left stroke) (B, C) Segment KLVFFAEN derived from Crystal aβ 16-26 D23N was used as a design target. The peptide inhibitor D1(magenta) model, D1(magenta), associated with the calculation target, THE KLVFFAEN (grey). The smaller D1 hydrophobic residues mimic the interactions with the fibile interface on one side of the peptide (B), while the other half of the peptide places large aromatic residues between Aβ residues, crushing any further interactions (C). (D) Overview of peptide inhibitors D and L amino acid conformation inhibitors D and L used in this study in amino acid conformations. Peptide LC is a D-form D1 L-form consultnepone and a negative control based on the peptide inhibitor D1 and its derivatives D1b and D1d. N.D., unspecified. E Peptide inhibitors D1, D1b and D1d reduce the cytotoxicity of Aβ1-42 dose-dependent, while the control peptide LC is not incubated at 10 µM Aβ1-42, incubated alone or with concentrations of different peptide inhibitors for 12 hours at 37 °C and then diluted with 1:10 pre-existing surface N2a cells. Cytotoxicity was measured by reduced MTT colour. Bars represent the average for individual technical replicates, with one standard deviation (n = 3-6; ns = not significant; **, p<0.002; ****, p<0.0001 using the usual one-way ANOVA Dunnett for the leftmost column). focused on these key features of the inhibitor jam in our second round design and aim to improve efficiency. We extended our peptides to expand more of our existing structures towards carboxy-terminus and changed conservative residues in the face that contained smaller hydrophobic residues. We picked out and tested six new designs. Of the six, eight amino acids were long, so the inhibitor would extend more across our crystal structure, which we called D1a-D1d. Two more, called D1e and D1f, were six amino acids long featuring a slight series of perturbations from D1 fail 1). Me Me two of the eight long amino acid inhibitors D1b and D1d, which were also effective in reducing the toxicity of AB1-42 by 10 times the ratio of surplus to equivalent (Figure 2 – Figure Supplement 1B,C). We then checked these two inhibitors, as well as in the range of D1 concentrations, with final concentrations ranging from 100 nM to 10 µM (Figure 2D, E). We found that all inhibitors induce a dose-dependent response, with all of which are estimated to be IC50 less than 1 µM. The six long-term residue inhibitors D1e and D1g also had similar effects to toxicity reduction as D1, but did not perform as well as D1 in the additional characterisation and were not further studied (Figure 3 – Figure 1B). Consultant negative peptide control, LC, inhibitor D1 L-form peptide, did not reduce toxicity (Figure 2E). Next, we tried to understand the mechanism by which our peptide inhibitors reduce the toxic effects of Aβ1-42. Therefore, we analyzed fibril formation to determine whether this reduction in toxicity can be explained by reduced aggregation. We incubated mole ratios of Aβ1-42 with our inhibitors 10:1, 1:1 and 1:10 and monitored the fibril formation with tioflavin-T (ThT) fluorescence at 37 °C quiescent conditions. We note that all of our inhibitors reduce fibril formation in a dose-dependent way, while negative control of peptide, LC, is not (Figure 3A, Figure 3-Figure Supplement 1A). Longer inhibitors, D1b and D1d, appear to be effective in the ratio of equivalents. However, when inhibitors are analysed at higher concentrations, they appear to be folding themselves but remain effective in reducing Aβ1-42 toxicity (Figure 3 – Figure 1C, Figure 2E). After 72 hours, samples were taken for TEM analysis of negative stains, which confirmed a decrease in the number of Aβ1-42 fibrils. D1b and D1d were more effective than D1 in reducing fibril formation, although all three inhibitors showed almost equal efficacy in reducing toxicity. Fibrils were observed in an equivalent molar ratio sample of Aβ1-42 and D1, while comparable samples D1b and D1d did not contain fibrils. Inhibitors that were not effective in preventing toxicity, such as D1a and D1c, were also less effective in blocking fibre formation (Figure 2–Figure 2– Figure 1C, Figure 3 – Figure 1A). (A) Peptide inhibitors D1, D1b and D1d reduce fibril formation of Aβ1-42, while negative control checkpeptide i LC is not. Fibril formation was monitored by ThT fluorescence. The curves indicate the average of the three technical replicates with one standard deviation below. B Negative stainTEM analysis confirms the results of thT analyses in Figure 3A. The samples were prepared as described above and incubated 72 hours prior to the TEM analysis. Images aβ1–42 to D1 (1:10), D1b (1:1) and D1d (1:1) were captured at 3200x; scale bars are 2 µm. All other images were captured at 24000x; scale bars are Nm. (C) Peptide inhibitors reduce the formation of a recognised Aβ1-42 formations of conformal monoclonal antibodies, while negative control peptides are not. The aliquots of the reaction were tested for antibody binding for 6 hours, 24 hours and 72 hours. The membranes were glued, as shown for clarity. oligomeene, not fibrils, are considered more toxic species Aβ (Lesné et al., 2006; Lambert et al., 1998; Benilova et al., 2012; Jin et al., 2011), we then examined whether our inhibitors affect the formation of oligomers or other cytotoxic Aβ1-42 species. We used body-building antibodies to probe samples of Aβ1-42 incubated by a 10-molar overuse inhibitor overnight at 37°C. Binding to all of our inhibitors with oligomer-specific conformation antibodies A11 and A11-O9 reduced all of our inhibitors (Figure 3C, Figure 3– Figure 1C, Figure 3 – Figure 2). Although we have not determined the exact oligomerical nodes of inhibitors are decreasing, our antibody binding data, together with the results of our toxicity tests, show that the formation of toxic oligomeria formation has decreased. In addition, inhibitors reduced the abundance of Aβ-conformations recognized by mOC24, mOC64, mOC104 and mOC116. These antibodies bind fibrillary plaques from the patient's AD tissue and/or 3xTg-AD mouse tissue (Hatami et al., 2014). In general, these results suggest that our inhibitors may reduce oligomers, as well as disease-related fibrillar body building. Since AD is only diagnosable long after Aβ aggregation is initiated, we do not know whether these inhibitors not only prevent amyloid aggregates from forming, but also if they can reduce the toxic effects of already formed aggregates. First, we incubated 10 µM Aβ at 37 °C for 12 hours to form oligomers (Figure 4-Figure Supplement 1A) and then added inhibitors at different concentrations immediately before adding N2a to cells and tested for toxicity with mTT color reduction. We found that the addition of an inhibitor to monomer Aβ1-42 was a significant difference from adding an inhibitor to premodified Aβ1-42 oligomers. In co-incubation with monomer Aβ, a shorter D1 inhibitor was as effective as D1b and D1d in reducing toxicity; however, only longer inhibitors D1b and D1d were effective when preformed Aβ kits were added to preformed Aβ kits (Figure 4A). Both longer inhibitors may completely relieve aggregate toxicity at 10 µM, but D1s are stronger by effectively reducing toxicity to 1 µM. D1b differs from D1d only at amino acid positions 6 and 7. We suspect that the difference in efficacy results from residue 6, since both inhibitors contain positively charged residues at position 7, but position 6 D1b is Gln while D1d is much bulkier Trp. peptide inhibitors may prevent the initiation of aggregation and block the toxicity of aggregated assemblies that appear to be more sensitive to mild disturbances in the composition of inhibitors. (A) Peptide inhibitors that reduce the toxicity of aβ1-42 aggregates already formed. 10 µM Aβ1 to 42 was incubated for 12 hours at 37 °C on its own. Incubated Aβ1-42 was added to the molar ratio indicated by the inhibitor and then diluted in 1:10 with previously plated N2a cells. Cytotoxicity was measured by reduced MTT colour. Bars represent the average with individual technical replicates (n = 3-6; ns = not important; ***, p<0.0005; ****, p<0.0001 using the usual one-way ANOVA-Dunnett for the leftmost column). B, C, C, c, inhibitors are associated with Aβ1-42 fibrils. (B) Peptide inhibitors do not distinguish between Aβ. 10 µM Aβ1 to 42 was incubated on its own for 72 hours at 37 °C. Peptide inhibitors were added with a 10-fold molar surplus and incubated at RT 24 hours prior to tem analysis. The images were captured in 24000x; scale bars are 500 nm. C) Inhibitor D1d binding is binding to fibrillary-Aβ1-42. The maximum response (RUmax) was derived by installing sensors in the d1d concentration range on a binding model with Kd of 52 ± 6 µM, which is displayed as a red line. These RUmax values are entered (mean ± SD, n = 3) as a concentration function and are installed on a one-to-one binding model that is displayed as a black line. We're following through with TEM to determine whether our inhibitors can lagregate fibers, or if the fibers are capped, as our inhibitor design would predict. We combined shaking conditions of 10 µM Aβ1-42 for 72 hours at 37 °C, then added inhibitors at 100 µM and incubated overnight. Since fibers still exist, we assume that our inhibitors are indeed capping or coating fibers in toxicity-inducing interfaces, thus preventing further sowing or toxic effects (Figure 4B). To investigate the clew capability of our inhibitors, we added inhibitors Aβ1-42 during the exponential phase of fibril growth (Figure 4-figure supplement 1B). We found that even with the lowest concentration inhibitor, 10 µM Aβ: 1 µM inhibitor, we see a minimal increase in signal inhibitors D1b and D1d. In addition, we noticed a slight decrease in ThT signal samples from a 1:1 inhibitor in addition, perhaps due to inhibitors replacing ThT molecules associated with fibrills. Since inhibitors prevent monomer aggregation (Figure 3A), we are wary of overinterpretation of the outcome of this test, since the inhibitor may be free of separating monomer or small nodes to fibrils. We performed SPR to check that our inhibitors bind to fibers. We find that the strongest aggregated assembly inhibitor D1d binds to Aβ1-42 fibrils visible Kd 52 µM (Figure 4C, Figure 4–Figure 2). To accommodate the data, we used a one-inhibitor-to-single-protein substrate model; but true Kd may be smaller due to the D1d self-interaction and polymorphic Aβ fibrils. Thus, we have shown that inhibitors D1b and D1d not only prevent the aggregation of monomeric Aβ, but also bind together with countries. After showing that our inhibitors block the toxic interface in Aβ, we questioned whether this interface could also be related to cross-seed tau. Firstly, we tried to confirm the direct sowing mechanism that others have announced (Guo et al., 2006; Miller et al., 2011; Vasconcelos et al., 2016). We tested the seeding of the tus, K18+ (244-380) microtubule binding domain in the ThT analysis at 37 °C shaking and found that Aβ1-42 and Aβ16-26 D23N fibrills sowed the aggregation, though not as effectively as the K18 fibrills (Figure 5A, Figure 5 – Figure 1A). This sowing effect was also observed in the presence of heparin in full-length tau (Figure 5 – Figure 1B). By contrast, K18 was unable to sow aβ (Figure 5 – Figure 1C). A) 50 µM tau-K18+ was sown with 10 % monomer equivalent for pre-formed fibriolia Aβ1-42, Aβ16-26 D23N or tau-K18 shaking at 700 rpm pbs. Fibril formation was monitored by ThT fluorescence. The error bars below show the average standard deviation of the three parallel technical samples. (B) Number of intracellular aggregates found in Tau-K18CY biosensor cells normalised by cells concentrated with seeds adding 250 nM tau40 or 250 nM Aβ1-42 fibrils. The error strips indicate the mean standard deviation of the technical replicates (n = 3; ****, p=0,0001 using the usual one-way ANOVA-Dunnett adentone in relation to the leftmost column and **, p=0,0028 for the Aβ vs. vehicle odd t test) (C) B imagery with a 10x magnification, scale of 100 µm. (D and E). Concentration-dependent sowing of a beta1-42 induced tau aggregation in tau-K18CY biosensor cells. D) Mean sowing of Aβ indicated as inhibitor concentration function. The error strips indicate the mean standard deviation of the technical replicates (n = 3; ns = not important; *, p<0.02; **, p<0.005; ***, p<0.001; ****, p<0.0001 using the usual one-way ANOVA-Dunnett in relation to the left column) and the dotted line indicates the average number of untreated Aβ1-42 fibrils.e aggregate. Representative images of E Tau-K18CY biosensor cells showing the concentration-dependent effect of D1b on sowing. The cells are shown at a 10X magnification, a scale bar of 100 µm. Next, we tested the immersion in an established HEK293 biosensor cell line, tau-K18 (P301S) EYFP, which becomes a microtubule binding domain tau P301S mutant. This cell line, referred to as tau-K18 biosensor cells, has been used to show prion as a seed transfected tau fibrils cells and has been used as a model system to test tau inhibitors (Seidler et al., 2018; Kfoury et al., 2012). We transfected biosensor cells tau40 or Aβ fibrils (Figure 4-figure supplement concentration of 250 nM. We found that Aβ was able to produce intracellular agregates significantly larger than the vehicle alone, but only about 2.5% of the effectiveness of tau40. It is not entirely surprising that Aβ is so low in the effectiveness of cross seeds; this reflects the previous result in a similar system (Vasconcelos et al., 2016). It is possible that tau fibrils contain several polymorphs and interfaces capable of homottypical seed, while Aβ may have a limited number of tau seed-competent body building. In vitro Aβ aggregation can produce a disproportionate number of kits compared to ad. Despite the fact that some Aβ species are tau seed. The conclusion that Aβ is indeed capable of seed aggregation tau-K18 expressing cell lines indicates that the cross-uht region of the tau is located in this microwind-binding domain. We found other amyloid protein fibrils and non-fibrillar Aβ are not heating-competent in this system (Figure 5-figure supplement 1D), which suggests a biosensor cell test can faithfully distinguish fibrills from amyloid proteins that differ from their underlying structures and sequences. If our inhibitors block the interface responsible for seeding, we expect that Aβ will be treated with more tau seeds. To test this hypothesis, we treated 250 nM Aβ fiber inhibitor at a concentration of 1 hour and transfected them with a biosensor cell line. All of our inhibitors were able to reduce seeding at 20 µM at the final concentration, while D1b showed a reduction in seeds at concentrations up to 1 µM (Figure 5DE). Although both D1b and D1d reduced Aβ cell toxicity, D1d was a more effective inhibitor of Aβ-toxicity, while D1b is a more effective inhibitor in reducing tau seeding. Next, we tried to verify that the Aβ region used in the design of inhibitors is important for the seeding of tau and that it can be directed by inhibitor D1b. We created two Aβ1-42 mutants with residues either disturbed by our steric zipper interface: Aβ1-42 L17R/F19R and Aβ1-42 K16A/V18A/E22A. We decided not to mutated the residue Phe20 because it has been observed in full-length structures in both buried and solvent-accessible interfaces (Lührs et al., 2005; Colvin et al., 2016; Gremer et al., 2017). We formed fibrils for each mutant build and natural type, then incubate them fibrils at the concentration of D1b, and use it as a seed tau-K18 biosensor of cells, as described above (Figure 5-Figure Supplement 2). We found that Aβ1-42 L17R/F19R fibrills were able to sow similar to WT Aβ1-42, while Aβ1-42 K16A/V18A/E22A was not detected. D1b inhibited the sowing of Aβ1-42 L17R/F19R, suggesting that residues K16, V18 and E2 create a seed interface directed by the inhibitor D1b. Our data support previous studies that suggest Tau binding to the surface of Aβ is a localized segment we decided and directed the design of aβ-aggregation and Aβ-mediated tau seed inhibitors (Guo et al., 2006; Miller et al., 2011). We suspecte that tau fibril may contain a similar self-improvement surface and would also be susceptible to treatment with our inhibitors. We first asked if Aβ inhibitors, D1, D1b and D1d can prevent monomeric tau aggregation. We did a ThT analysis of 10 µM tau40, shaking at 37°C and 0.5 mg/ml heparin and found that all inhibitors act in a dose-dependent way similar to our results with Aβ monomer, while control inhibitor LC does not reduce tau aggregation (Figure 6A, Figure 6-Figure 1A). Peptide inhibitors are not able to block amyloids, which form proteins hIAPP or alpha synuclein, which indicates that these inhibitors are specific to Abeta and tau, and are not generic amyloid inhibitors (Figure 6-figure supplement 1B). (A) Peptide inhibitors D1, D1b and D1d reduce the formation of tau40 fibril. The 10 µM tau40 monomer was incubated at 1:10, 1:1 or 10:1 with a molar ratio of 0,5 mg/ml heparin at 700 rpm at 37 °C for each inhibitor. Fibril formation was monitored by ThT fluorescence. The plots shall have an average of three technical replicates with one standard deviation below. (b) and (c) and (c) Effect of inhibitors on the sowing of tau40 fibrils in tau-K18CY biosensor cells. The cells were sown with 250 nM tau40 fiber (final concentration); tau40 fibres were incubated at the final concentration indicated by the peptide inhibitor within one hour before the addition to the cells. (B) The average number of aggregates at the inhibitor concentration indicated, bars represent the average for individual technical replicates, the error bars have one standard deviation (n = 3; ns = not significant; *, p<0.03; **, p<0.023; ***, p<0.0008; ****, p<0.0001 using the usual one-way ANOVA- Dunnett left column). the dotted line represents the number of unprocessed tau40 fibrils aggregates. The IC50 value was calculated from the dose response plot of the inhibitor D1b (C). Representative images of the effects of D1b seeding. The cells are shown at a 10X magnification, a scale bar of 100 µm. (D) The seeding of tau interface mutation fibrills in tau-K18CY biosensor cells is reduced by D1b. The average number of aggregates indicated at inhibitor concentration, bars represent the average for individual replicates of technical samples, the error strips have one standard deviation (n = 3; ns = not significant; ****, p<0.0001 using the usual one-way ANOVA-Dunnett in relation to the leftmost column). we had observed differences in the effectiveness of inhibitors in monomer and Aβ aggregated species, we examined whether the inhibitor was effective against the seeding capacity of tau40 fibrils. We formed tau40 fibrils, treated them with the concentration of the inhibitor shown and transfected into tau-K18 cells to measure inhibition of sowing. We found that similar to our Aβ-mediated tau biosensor seed experiment, D1b, was the best inhibitor, ic50 4.5 µM. D1 was slightly effective, while D1d showed a reduction in seeding only when increased to 75 µM (Figure 6B,C). It may be that D1b plays twice to inhibit both Aβ and tau, and this combined effect could explain the drastically reduced seeding from Aβ fibrils in our previous experiment (Figure 5D). Next, we tried to identify possible binding sites for Tau for D1b. We identified that the regions knew that tau aggregation leaders could share structural properties with the AB core and thus inhibit it with d1b. We designed tau40 mutants that interfere with the main anti-acting stericziper interfaces designated by VQIINK (Seidler et al., 2018) and VQIVYK (Sawaya et al., 2007) and AD tau fibrils (Fitzpatrick et al., 2017) with cryoem models. In total, we tested six different structures, each designed to block all but one tau aggregation interface. The first three mutants were designed to block VQIVYK aggregation interfaces in addition to all, excluding all, excluding all of the three known VQIINK interfaces. Mutant 1 (Q276W, L282R, I308P) leaves only interface A VQIINK available for aggregation, mutant 2 (Q276W, I277M, I308P) leaves only interface B for aggregation and mutant 3 (I277M, L282R, I308P) leaves only the interface available for C aggregation. Constructions 4 and 5 were designed to test the effects of blocking VQIINK and all vQIVYK surfaces. Mutant 4 (Q276W, I277M, L282R, Q307W, V309W) leaves only the vQIVYK dry interface available for aggregation and mutant 5 (Q276W, I277M, L282R, I308W) leaves only the solvent available for surface aggregation. In addition, we tested the effect of D1b on blocking sowing using 3R tau, which does not have a VQIINK aggregation segment and leaves the VQIVYK interface intact (Figure 6D, Figure 6 – Figure 2C-E). To test whether D1b inhibits specific interfaces, fibrils were formed from all different mutants and then both were incubated at D1b concentrations and used to sow natural tau-K18 biosensor cells, as previously described in wild type tau fibrils (Figure 6 – Figure 3A,B). We found that D1b was most effective in inhibiting the seeded fibrils mutants, which left intact: the interface a VQIINK, which is thought to involve the aggregation of site I277 tau, the solvent available for interface VQIVYK as well as 3R tau (Figure 6D). D1b also moderately inhibited several other tau mutants, but required high seed-suppressing concentrations (Figure 6 – Figure 2C). As a check, we tested the seeding of 40 mutants, which combined all the different mutations, and found that this mutant did not cause seeding in the cells of the ta-K18 biosensor (Figure 6 – Figure 6 – Figure Supplement 1E), despite fibrils incubation with heparin, indicating that at least one known is necessary for sowing. The control inhibitor LC does not affect the sowing of any structure at the slightest (Figure 6 – Figure 1F). In total, these data show that D1b inhibits both tau VQIINK and VQIVYK aggregation segments and shows that everyone can have common structural properties with the Aβ core, which allows Aβ to cross-seed tau. Amyloid polymorphs may vary depending on whether they are concentrated in vitro or extracted from human brain tissue (Falcon et al., 2018). We tried to determine whether our inhibitors were capable of blocking pathological forms of either tau or Aβ. As previously suggested in our physical antibody analysis and structural intoxication (Figure 3C), let's assume the hypothesis that our inhibitors block disease-related amyloid polymorphs. Since we also found that our inhibitors blocked both homotypical and heterocellular tau seeding by aggregated tau and Aβ, we tested our inhibitor series of raw lysate from AD to the donor patient's brain tissue. We homogenized tissue from three brain regions in one AD patient's brain, the hippocampal region, affected early, as classified in Braak staging, and in the lobe and occipital lobe regions that are affected later by disease progression (Brier et al., 2016; Schwarz et al., 2016). We also produced samples from the patient's tissue with progressive supranuclear paralysis (PSP), a disease of tau aggregation that did not reveal Aβ aggregation by immunostaineation. We produced samples of untreated patient tissue, as well as tau-immunodegradable PSP tissues. We transfected the brain by lysing into biosensor cells; 10 µM D1, D1b or D1d. We found that treatment of lysates from the brain with D1b significantly reduced sowing with all samples of brain tissue studied (Figure 7). The total load of tau of different tissues has not been verified and this is probably the cause of different reasons for seed efficiency, which are considered in different tissue types. Although our inhibitor D1b showed a reduction in hippopotamus seeding, the fibril load in the area may have been too high to be effectively stopped by the dose used. Interestingly, PSP tauopathy tissue was also a sensitive treatment for any inhibitors, d1b displaying the most pronounced inhibition. We assume that D1b recognizes a common toxic epitope found in both Aβ and various tau polymorphs. Brain lysate was prepared as a TBS buffer in three brain regions of one AD patient, and from one sample to a PSP the patient lacks Aβ spots. Brain lysate non-disease patient (neg cntl) and tau immunodepleted sample PSP tissue are on the right panel. The cells were sown with 1/400 dilution of lysate in brain tissue; inhibitors were incubated overnight with a lysing inhibitor before being added to cells. A concentration of 10 µM peptide was used for all indicated tests. (A) Medium lysosa from each brain, with or without the addition of inhibitors. Bars are average with individual technical replicates (n = 3; ns = not significant; *, p<0.05; ***, p<0.0005; ****, p<0.0001 using the usual one-way ANOVA-Dunnett in relation to the left column). B) A representative representation of seminal biosensor cells, shown at a 10X magnification bar of 100 µm. Extended ANOVA data included as an additional file. search for stunning targets AD is muddy with numerous proteins involved and a lack of understanding of whether two histological protein traits, Aβ and tau, interact directly with each other. In addition, Aβ, an obvious initiator of disease, aggregates into a wide variety of species, from soluble oligomers from dimers to those containing dozens of copies, to polymorphic fibril deposits. While there may be many toxic fabrics that target a specific complex or structure with a toxic motif that exists in various these manufactures could be an effective strategy for designing pharmaceuticals. We target the amyloid core segment of Aβ due to its defined amyloidogenicity, and the putative interaction of late aggregation protein, tau. In our efforts, we focused on the Aβ16-26 segment with hereditary mutation D23N, the structure of which was determined by MicroED. While this segment's crystalline structure is fibril-like, and similar to the previously observed zipper interface as well as the interface of full-length fibrils, the out-of-register interface β-strands indicates that parts of this body structure may be present in a number of toxic oligomeral intermediates as well as fibrils. We successfully used this structure to design a number of related inhibitors that reduce the toxicity of the Aβ model of N2a cells. Our biochemical and toxicity studies show that these inhibitors work in two ways. The first is preventing monomeric Aβ from aggregation. The second is a pre-formed reduction of the toxicity of

oligomeric Aβ, which can bind and block the surface responsible for toxicity or sowing. While all of our proposed inhibitors prevent monomeric Aβ from aggregation, only longer D1b and D1d versions are effective in reducing the toxicity of preformed nodes. These two peptides were designed by extending the C-terminus. D1b and D1s can conceivably act by concealment to provide toxicity, supported by early-onset hereditary mutations that converge on residues 21-23 (Lazo et al., 2009; Krone et al., 2008; Chong et al., 2013). Our data is related to the extended Aβ nucleus spread of the disease, because targeting inhibitors in this region seem to block the tantalizing interface needed for crossseed tau. Aβ fibers treated with D1b showed the formation of cross-seed in ta-K18 biosensor cells. Tau fibres treated with D1b showed similarly inhibited biosensor cells. The dual efficacy of the inhibitor D1b, designed for the Aβ 16-23 region, suggests that these two pathological aggregates Aβ and tau have a common structural motif in AD. Indeed, we find that solvent-accessible residues K16, V18 and E22 Aβ are important for tau sowing. By contrast, using mutant structures tau only one available amyloid interface, we were able to determine two interfaces of tau where seeding was very reduced in D1b. Both R2 and r3 amyloid-prone regions of tau contain D1b sensitive interface. It should be noted that the R2 surface blocked by D1b contains ice I277, which has previously been found to be critical for tau aggregation (Kirschner et al., 1986). We find that the transfer of the crystal structure of our Aβ segment to the structures of tau R2 and R3 shows a high degree of structural similarity both in the spine and probably in the complementarity of the lateral circuits to be intrinsically intertwined (Figure 6 – Figure 3). Interestingly, Aβ layers well into these regions of the tau both parallel and anti-parallel orientations, indicating that either fiber or smaller oligomers could be able to cross the heating ends of fibrils. Another seed may be facilitated on the side of the Aβ fibril using solvent-accessible interfaces from residues 16 to 22 (Figure 6 – Figure 4). Although the modeled interface tau is calculated as a form of favorable energy, the burial of polar and charged residues (TauQ307/AβK16) can cause this interaction to be transient. In addition, differences between the overall structure and stacking of the two fibrils may explain why fibrils containing both Aβ and tau fibrils are not followed. On this basis, it is recommended that Aβ and VQIINK and VQIVYK amyloid core may form similar structures in AD that are biochemically capable of crossseed. In line with our conclusion that the regions of Aβ and tau share structural similarities, we found that Aβ inhibitor D1b is able to reduce the sownment of homogenates in the brain, indicating that the inhibitor recognizes the structural motif associated with the disease, while D1 and D1d are much less effective. It is strange that seeding both AD and PSP is a significantly reduced inhibitor of D1b, as psp pathology does not contain Aβ aggregates. It is thought that different phenotypes of the disease, which have different fiber morphologies, commonly called strains, are determined by the formation of different steric-zipper cores (Sanders et al., 2014). Thus, PSP fibers may contain a different nucleus than our in vitro aggregated tau or AD derived tau. However, our tau mutagenesis results suggest that inhibitor D1b can be felt in at least two unique core interfaces, and thus could be able to operate multiple strains of fibers. Other fibril polymorphs with different structural conforms that are not sensitive may occur. In addition, it is not known how different co-factors and translational modifications, such as tau phosphorylation, may affect Aβ's ability to seed tau and thus D1b. Cross-seeding of Aβ can be one of many possible incentives to merge tau. As with other peptide-based amyloid inhibitors, the effective dose for reducing the toxicity of aggregated species is greater than the deferral of monomer aggregation. This is underlined by the different effectiveness of our series of related inhibitors, where some inhibitors were able to avoid initial aggregation, but not toxicity or sowing from different assemblies. It seems that inhibitors that prevent the addition of the nucleus are much more indiscriminate than those that alleviate toxicity by linking to a separate structure. This trend was observed in both Aβ and tau, which refers to a common inhibitory mechanism for both proteins, and underlines the need for a number of experimental measures to validate the efficacy of the inhibitor. Overall, our results show that direct interaction between Aβ-nucleus and tau amyloid-prone regions facilitates cross-seeding. Our inhibitors designed for the Aβ nucleus segment to prevent cross-seeding, as well as tau homotypical seed. The intertwined nature of these two proteins in the AD suggests that the treatment of the disease requires control of the aggregation of both. Early detection remains important, but this data provides a platform for additional inhibitors to be designed to inhibit the optimised spread of amyloids associated with amyloids in Alzheimer's disease. Reagent typeDesignationSource or referenceIdentifiersAdditional informationCell line (Homo-sapiens)HEK293 -K18 (P301S)-EYFPDiamond LaboratoryCell line (M. musculus)Neuro-2a cell lineATCCCat # CCL-131 RRID:CVCL_0470AntibodyGoat anti-Mouse IgG H and L (FITC) secondary antibodyAbcamCat# ab7064, RRID:AB_955234WB 1:10000AntibodyDonkey anti-Rabbit IgG H and L (FITC) secondary antibodyAbcamRRID:AB_955259WB 1:10000AntibodyA11 (rabbit polyclonal)MilliporeCat# AB9234 RRID:AB_11214948WB 1:500AntibodyOC (rabbit polyclonal)MilliporeCat# AB2286 RRID:AB_1977024WB 1:2000Antibody6E10 (mouse monoclonal)BioLegendCat# 803003, RRID:AB_2564652WB 1:5000AntibodyA11-09 mOC 64 mOC 24 mOC 116 mOC 104(rabbit monoclonal)Glabe Laboratory, AbcamWB 1:100Peptide, recombinant proteinRecombinant Amyloid Beta 1–42 (pET15b-MBP-AB)This paperSee Materials and methods sectionPeptide, recombinant protein(D)-LYIWVQGenscript>95% purityPeptide, recombinant protein(D)-LYIWIWRTGenscript>95% purityPeptide, recombinant protein(D)-LYIWIQKTGenscript>95% purityPeptide, recombinant protein(L)-LYIWVQGenscript>95% purityPeptide , recombinant proteinRecombinant Tau40 (1-441, pET22b)This paperVt materials and methods sectionPeptid, recombinant proteinRecombinant K18(244-372) K18+ (244-380) (PNG2)This paperVt materials and methods sectionPeptid, recombinant protein KLVFFAENVGSGenscript>98% purity chemical compound, bromide (MTT) dyeSigmaCat # M5655Gemic compound, drugThioflavinTSigmaCAS ID: 2390-54-7Software, algorithmXDS SCR_015652Software, algorithmCCP4 SCR_007255Software, algorithmPHENIXPMID: 20124702 RRID: SCR_014224Model building and improvementSoftware, algorithmCootPMID: 20383002 RRID: SCR_014222Model buildingSoftware, algorithmRosetta SCR_015701Software, algorithmGraphpad PrismGraphPad Priism ( )RRID:SCR_015807Version 8Soft, algorithmImageJImageJ (RRID:SCR_003070Software, algorithmFoldit SCR_003788 Request detailed protocol for Aβ and interface mutants, cleaned krotee et al. (2018). After cleaning, the protein was lyophilised. Dried peptide powder was stored in desiccant cans at -20°C. The application for detailed protocol candidate inhibitors were custom made and purchased by Genscript (Piscataway, NJ). Lyophilised candidate inhibitors were reconstituted at 10 mM at 100% DMSO. 10 mM stocks were diluted as necessary. All stocks were kept frozen at -20 °C. Amyloid Beta was prepared by reconstitution of lyophilised peptide in 100% DMSO or 100 mM NH_4OH. The sample was then filtered with a centrifuged sample and the concentration was evaluated by BCA analysis (Thermo Scientific, Grand Island, NY). DMSO or NH_4OH peptide stocks were diluted 100 times filtersterized by Dulbecco's PBS (Cat. #14200-075, Life Technologies, Carlsbad, CA). Apply for detailed protocol 16-Ac-KLVFFAENVGS-NH3-26 (Aβ 16-26 D23N) dissolved at a dose of 4.5 mg/ml in 20% DMSO. Microcrystals were grown in a lot of 0.2M magnesium format, 0.1M Tris base pH 8.0 and 15% isopropanol at room temperature under quiescent conditions. Crystals increased for 4 days up to a maximum of 2 weeks. The detailed protocol for microed data collection and processing procedures is largely in line with published procedures (Shi et al., 2016; Hattne et al., 2015). In short, a 2-3 µl drop of crystals suspension was placed onto the Quantifoil holey-carbon EM grid then blotted and glazed plunging into liquid ethane using vitrobot Mark IV (FEI, Hillsboro, OR). Blotting times and forces were optimized to keep the desired concentration of crystals at an age and avoid damaging crystals. The frozen nets were then immediately transferred to liquid nitrogen storage or placed in the Gatan 626 cryo-holder for shooting. Images and diffraction patterns were collected from crystals using the FEI Tecnai 20 TEM with field emission weapon (FEG) running at 200 kV and equipped with a bottom mount TVIPS TemCam-F416 CMOS-based camera. Diffraction patterns were recorded by running the detector in video mode using an electronic rolling × 2 pixels with binning (Nannenga et al., 2014). The exposure times of these images were either 2 or 3 s frame During each exposure rotated continuously one-way at a fixed rate of 0,3 degrees per second at an electron beam corresponding to a fixed angle wedge of 0,6 or 0,9 degrees per frame. Crystals that appeared visually undistorted produced the best diffraction. The data sets for individual crystals were merged to improve completeness and aggregation. Each crystal data set included a reciprocal space wedge between 40° and 80°. We used a selected aperture with an illuminating spot size of approximately 1 µm. The geometry described above is equal to the electron dose rate of less than 0.01 $e^-/Å^2$ per second deposited on our crystals. The measured diffraction images were converted from TIFF to SMV crystallography format using commonly used software (available for download . We used XDS to index diffraction images and XSCALE (Kabsch, 2010) to connect and scale together datasets from thirteen different crystals. We are requesting a detailed protocol We determined the structure of Aβ 16-26 D23N using molecular replacement. KLVFFA (PDB 2Y2A) led us to our atomic model. The solution was obtained by Phaser (McCoy, 2007). The following model construction and refining rounds were carried out with COOT and Phenix respectively (Emsley and Cowtan, 2004; McCoy et al., 2005). Electron dispersion factors were used for refining. Some discussions extended to the 1.40 Å resolution. The calculations of the buried area and Sc were carried out together with AREAIMOL (collaborative calculation project, 1994; Lee and Richards, 1971) and Sc (Connolly, 1983; Lawrence and Colman, 1993; Richards, 1977). Request a detailed protocol for computational designs performed using RosettaDesign software as described above (Sievers et al., 2011). The atomic structure of the 16-KLVFFAENVGS-26 Aβ segment was used as a baseline template for the calculation design. At the end of the source template of the atomic structure, an expanded L-peptide (or D-peptide, six to eight residues) was first placed at the end of the source template. The design procedure was then built into the side circuit of all residues placed on the spine of nine residues of the peptide placed on the growing end of the fibrils. The optimal number of rotamers was identified as those that minimize the energy function, which includes lennard-jones potential, orientation-dependent hydrogen bond potential, insult term, amino acid-dependent reference energies, and statistical toration potential, which depends on the spine and the dihedral corners of the lateral circuit. The calculations of complementarity between the buried area and the shape were carried out in combination with areaimooli and Sc4 from the set of crystalgraphic programmes (collaborative com working project, 1994). The solubility of each peptide was assessed by the hydropathy index (Kyte and Doolittle, 1982). The proposed peptides were selected on the basis of the binding energy, complementarity of shapes and peptide solubility calculated in the upper or lower binding mode. Each structural model The peptides underwent human control using pymol, which excluded those peptides with sequence excess and less binding interactions. Eventually, the selected peptides were synthesized and tested experimentally. Request detailed protocol Aβ1-42 dissolved and diluted as previously described. Inhibitor stocks were prepared at 100% DMSO and added to include a 10 µM monomer Aβ1-42 inhibitor-determined ratio with a final concentration of 1% DMSO. The samples were incubated for 72 hours at 37 °C under quiescent conditions. Aβ1-42 fibrils were formed as described and then treated with the indicated inhibitor ration for 24 hours at 37°C under quiescent conditions. Fibril abundance was checked using electron microscopy. Request a detailed protocol samples were spotted on non-holey networks and were left at 160-180 s. The rest of the liquid was wicked out and then left to dry before analyzing. Tem samples of negative stains were treated with 2% uranyl acetate after the sample was vicious out of the net. After one minute, the uranyl acetate was vicious. The nets were analyzed using the T12 Electron Microscope (FEI, Hillsboro, OR). The images were collected at a magnification of 3200x or 24000x and were recorded with a 2k CCD camera × Gatan 2k. Request detailed protocol thioflavin-T (ThT) tests performed with black polystyrene 96 salival plate (Nunc, Rochester, NY) or black polypropylene 96 borehole boards (Greiner Bio-One, Austria) as shown and sealed with UV optical tape. The total response volume was 150 µl per well. Aβ1-42 was prepared as described. Inhibitors were added at accused concentrations with a final concentration of 1% DMSO. ThT fluorescence was recorded by excitation and emission of 444 nm and 482 nm, respectively, using Varioskan Flash (Thermo Fisher Scientific, Grand Island, NY). The tests were carried out at 37 °C without shaking in three copies and the readings were recorded every 5 minutes. This forest analysis included a 10% monomer equivalent to preformed fibrils, aggregated LoBind polypropylene tubes, and sonicated for 10 minutes before adding. Inhibitor interruption analyses were prepared according to the above on polypropylene plates. At approximately T1/2, readings were stopped and inhibitors were added as indicated, and the plates were refrosted with a new UV optical tape. The analyses with Tau40 were prepared as follows: 0,5 mg/ml heparin (Sigma Cat No. H3393) was added to the reaction mixture and the tests were carried out at 37 °C with a double orbitoksad at 700 rpm. The K18+ studies were prepared as follows: The tests were carried out at 37 °C with double orbital shaking at 700 rpm on polypropylene plates. The seeding analyses included 10% monomer equivalent preformed fibrils, sonicated 10 minutes before inclusion. Request detailed protocol for Neuro2a (N2a) cells (ATCC cat #CCL-131) were cultured mem media (Cat. #11095-080, Life Technologies) plus 10% fetal bovine serum and 1% pen-strep (Life The cells cultured at 37 °C in a 5% CO_2 incubator. The cells were authenticated by COX I Gene Analysis (Laragen) and mycoplasma negative MycoAlert PLUS Detection Kit (Lonza, cat #LT07-701). To request a detailed protocol, N2a cells were surfaced in 5,000 cells per well on 90 µl growing medium, clear 96-well plates (Cat. #3596, Costar, Tewksbury, MA). The cells were allowed to hold the plate for 20-24 hours. Samples from Aβ1 to 42 were incubated at 10 µM with or without inhibitors, with a different ratio of 12 hours at 37 °C and then transferred to N2a cells. 10 µl of the sample was added to the cells. In doing so, the samples were diluted in 1/10 of the in vitro stocks. The experiments were done in triplicate. After 24 hours of incubation, 20 µl of thialylal blue tetrazolium bromide MTT dye (Sigma, St. Louis, MO) was added to each well and incubated under sterile conditions for 3,5 hours at 37°C. The MTT color margin is 5 mg/ml dulbecco's PBS. The plate was then removed from the incubator and the MTT analysis was stopped, carefully removing the growing medium and adding 100 µl 100% DMSO to each well. The absorption was measured at 570 nm by SpectraMax M5. The background reading was recorded at 700 nm and then subtracted from the 570 nm value. Only carrier-treated cells (PBS+0.1% DMSO) were designated 100% viable and cells treated with 100% DMSO declared viable, and the viability of all other treatment cells was calculated accordingly. We used one-way ANOVA for our importance as a statistical test. Extended ANOVA data included as an additional file. Graphpad Prisma's four-parameter nonlinear dose-response curve was used to evaluate IC50 values. The detailed protocol Aβ1-42 samples were incubated at 10 µM with or without inhibitors for 6, 24 and 72 hours at 37 °C and were observed on nitrocellulose membranes (Cat. # 162-0146, BioRad, Hercules, CA). 20 µl was loaded for each condition; 2 µL is observed at the same time and allowed to dry between use. The membranes were slotted as previously described (Krotee et al., 2017), except for the primary antibodies used. Previously, antibodies used in the analysis (Hatami et al., 2014) were developed and characterised. Blots was quantified by ImageJ. The request for a detailed protocol for SPR tests was conducted using the BiacoreT200 instrument (GE Healthcare). Aβ42 fibrils/tau K18 fibrils were immobilized CM5 sensor chip. The Aβ42 fibrills were prepared by placing 50 µM Aβ42 samples of PBS pH 7.4 into two wells Nunc 96-well optical lower plate (Thermo Scientific), 150 µl/well and incubating the plate in a microplate reader (FLUOstar Omega, BMG Labtech) at 37 °C with double orbital shaking at 600 minutes overnight. The sample taken from the two wells was aggregated and the Aβ42 fibrils were separated from the incubation mixture by centrifuged at 13 000 xG, at 4 °C for 45 minutes. The supernatant was removed and the pellet was resold in equal amounts as a PBS supernatant. Insulated fibrils sonicated using a probe sonicator 1-2 min 18% amplitude 2 s in, 5 s off impulses. Ultrasonically treated fibrils were filtered through 0.22 µ filter to remove large aggregates. Sonicated and filtered fibrils were diluted in 60 µg/ml 10 mM NaAc, pH 3 and then, immobilized immediately by cm5 sensor chip using standard amine coupling chemistry. In short, carboxylic groups were activated on the sensor surface by injecting 100 µl 0.2 M EDC and 0.05 M of NHS mixture from flow cells 1-2. Fibrils were then injected at a flow rate of 5 µl/min over the activated sensor's surface flow rate over 2 900 s. The remaining activated groups in both flow cells were blocked by injecting 120 µl 1 M ethanolamine-HCl pH 8.5.. For binding analysis, each peptide inhibitor was dissolved at 100% DMSO at a concentration of 1 mM and diluted in pH phosphate buffer in pH to 7.4+ 1.2% in DMSO at a concentration ranging from 5 µM to 260 µM. Each peptide was injected at a flow rate of 30 µl/min above both flow cells (1 and 2) at an increase in concentration (running buffer, PBS, pH 7,4+1,2% DMSO) at 25 °C. For each sample, the exposure time and dissociation time were 120 s and 160 s. 3 M NaCl respectively was used as a regeneration buffer. The data were processed and analysed using Biacore T200 evaluation software 3.1. Flow cell 1 (blank control) data were subtracted from flow cell 2 data (immobilized fibrils/monomers). The equilibrium dissociation constant (Kd) was calculated by installing a 1:1 binding model (equation 1) in relation to the peptide concentration (C) of the steady state peptide binding level (Req). Rmax = binding volume of the analyte surface RI = bulk refractive index contribution in sample Request detailed protocol K18, K18+, Human Tau40 (residues 1-441) WT, 3R and mutants: interface A (Q276W, L282R, I308P), interface B (Q276W, I277M, I308P), interface C (I277M, L282R, I308P)interface 1 (Q276W, I277M, L282R, Q307W, V309W), interface 2 (Q276W, I277M, L282R, I308W), were expressed in pET2 8b The His-tag (tau40) or PNG2 (K18, K18+) TERMINAL C in BL21-Gold E. coli cells grown in TB OD600 = 0,8. The cells were induced at 0,5 mM IPTG for 3 hours at 37 °C and milked by ultrasound 50 mM Tris (pH 8.0) 500 mM NaCl, 20 mM imidazole, 1 mM beta-mercagaethanol, and HALT protease inhibitor. The cells were washed by sonication, explained by centrifugation at 15,000 rpm for 15 minutes, and further over 5 ml of TheTrap affinity column. The column is washed with a lysis buffer and eluted at the imidazole inclination of 20 to 300 mM. Purified fractions containing Tau40 were washed into a 50 mM MES buffer (pH 6.0) with 50 mM NaCl and 1 mM beta-mercaptoethanol and cleaned by cation exchange. Top fractions polished HiLoad 16/600 Superdex 200 pg 1X PBS (pH 7.4) and concentrated ~ 20-60 mg / ml ultrafiltration using 10 kDa cutoff. Request detailed protocol Aβ fibrils was prepared at 200 µM at 37 °C 72 hours before dilution 50 µM PBS (pH 7.4) for sowing tests. Tau40 WT and interface mutation fibrills were prepared by shaking 50 µM tau40 in the PBS buffer (pH 7,4) with 0,5 mg/ml heparin (Sigma Cat No. h3393) and 1 mM dithiotritol (DTT) for 3-6 days. Fibrillization confirmed the endpoint of the reading, and fibrills were then diluted to 20-25 µM OptiMEM (Life Technologies, cat no. 31985070). Inhibitors dissolved in DMSO were added 20 µl of diluted fibrils at a concentration 20 times higher than the final desired concentration. Fibrils were incubated with ~16 hr inhibitor, and then were sonicated in cup horn water bath for 3 minutes before sowing the cells. The resulting pre-capped fibrills were mixed with one volume Of Lipofectam 2000 (life technologies, cat No 11668027) prepared by diluting 1 µl of lipofecta in 19 µl OptiMEM. After 20 minutes, 10 µl of fibrils was added to the cells of the tau-K18CY biosensor to achieve the final ligand concentration. The cells were controlled by STR profiling and confirmed mycoplasma negative (Laragen). The quantitative determination of seeding was determined by photographing the entire well of a 96-hole plate, sown in triplicate and depicted in the YFP channelceligo image by the cytometer (Nexcelom). The aggregates were read using ImageJ (Eliceiri et al., 2012) by subtracting the background from the seedless cells of fluorescence and then counting the number of peaks above the fluorescence background using a built-in particle analyzer. We used one-way ANOVA for our importance as a statistical test. Extended ANOVA data included as an additional file. Dose-effect curves were designed for inhibitor peptides with concentration dependence, matching graphpad prism with a nonlinear regression model. High-resolution images were obtained using the ZEISS Axio Observer D1 fluorescent microscope. The request for a detailed protocol for human brain tissue was obtained in a neurology laboratory at UCLA Medical Center. The AD and PSP cases were confirmed by the Neurology Laboratory's immunostaining dissected brain tissue sections, and the PSP donor confirmed that there is no amyloid immunonoreactivity. These tissue sections of the brain regions were homogenized manually using the single-use ultra-tissue mill (Thermo Fisher) in TBS (pH 7.4), plus a 1X HALT protease inhibitor. Homogenized tissue was defeated on several PCR tubes and prepared for sowing in biosensor cells by ultrasound, as described in Kaufman et al. (2017), except for tissue sections sonicated twice for more than 2 hours in an ice-cooled circulating water bath, where individual sample tubes are mixed to ensure that each tube receives the same sonication energy. Seeding into biosensor cells was then measured by transfecation and quantified as described above. We used one-way ANOVA for our importance as a statistical test. Extended ANOVA data included as an additional file. Request detailed lysate protocol as described above. 2 µg (0.2 µl 11 µg/ul) Tau antibody (Dako A0024) was conjugated with 0.75 mg proteing-dynabeads (25 µl 30 mg/ml). The antibody was mixed with beads and was smarted for 10 minutes, washed with 200 µl citrate-phosphate wasp pH 5.0 and then resusprated in a minimum amount of the washing buffer. 200 µl of lysate 1/20 of the brain diluted in OptiMEM was added to the suspension with antibody beta and nutated for 30 minutes. The supernatant was removed and used in transfection biosensor cells as described above. Request a detailed α-synapsine was expressed and cleaned as described in rodriguez et al. with the following exceptions to the expression protocol. Overnight starter culture was grown 100 ml, 7 ml instead of 15 ml, of which 7 ml was used to inoculate 1 L. After induction, cells were allowed to grow for 3 to 4 hours at 34 °C (4 to 6 hours at 30°C). The cells were then collected in centrifuges at a rate of 5,000 x g. α tht-analyses of black 96-well plates (Nunc, Rochester, N.Y.) with sealed UV optical tape. The total response volume was 180 µl per well. ThT fluorescence was recorded by excitation and emission of 444 nm and 482 nm, respectively, using Varioskan Flash (Thermo Fisher Scientific, Grand Island, NY). The tests were carried out at 37 °C, shaking 600 rpm with teflonbed, in triplicate and the readings recorded every 15 minutes. Synapses 105 µM alfa were diluted to a final concentration of 50 µM 25 µM tioflavin-T and PBS. Inhibitors were added to a specified concentration by diluting 10 mM stocks 100% DMSO 1 to 40 in the same way. Thus, inhibitors were tested 5:1 molar over α-synapsine. Request a detailed protocol for Human IAPP1-37NH2 (hIAPP) purchased in Innopep (San Diego, CA). Peptides were prepared by dissolving the lyophilised peptide at 100% 1,1,1,3,3,3-hexafluoro-2-propanol (HFIP) for 250 µM for 2 hours. The sample was then spin-filtered and then THE HFIP was removed from the CentriVap concentrateor (Labconco, Kansas City, MO). After removal of HFIP, the peptide was dissolved at 1 mM or 10 mM in 100% DMSO (IAPP only) or 100% DMSO solutions containing 1 mM or 10 mM inhibitor. DMSO peptide stocks were diluted 100 times by filtersterized Dulbecco's PBS (Cat. #14200-075, Life Technologies, Carlsbad, CA). Tioflavin-T (ThT) analyses with hIAPP were made with black96-well plates (Nunc, Rochester, N.Y.) sealed with UV optical tape. hIAPP1-37NH2 and mIAPP1-37NH2 prepared as described. The total response volume was 150 µl per well. ThT fluorescence was recorded by excitation and emission of 444 nm and 482 nm, respectively, using Varioskan Flash (Thermo Fisher Scientific, Grand Island, NY). The tests were carried out at 25 °C without shaking in three copies and the readings were recorded every 5 minutes. The detailed protocol Aβ 16-26 and the structural superposition of tau (5V5B, 6HRE) were carried out using LSQ from coot (Emsley and Cowtan, 2004). We calculated the square mean (RMSD) 6 to 8 for parallel residue orientations. The calculation of the LSQ against the parallel LSQ of Cα atoms Aβ 16-22 and tau 275-281 (5V5B) and the rotations of the chain of communication were optimised with Foldit (Kleffner et al., 2017) over 2000 iterations to reduce energy to -603 REU. For the lateral sowing model, residues of Aβ(5OQV) were added to 16 to 21 Tau (6HRF) 304 to 309. Tau was then manually moved perpendicular to the fibril axis to make an additional surface 5OQV. Foldit optimized the spine and side circuit rotation to reduce energy to -1517REU. 1 2 3 4 5 6 7 8 9 10 11 12 13 14 15 16 17 18 19 20 21 22 23 24 2 26 27 28 29 30 31 32 33 34 35 36 37 38 39 40 41 42 43 44 45 4 6 47 48 49 50 51 52 53 54 55 56 57 58 59 60 61 62 63 64 65 66 67 68 69 70 71 72 73 74 75 76 77 Thank you for your article Amyloid Beta nuclear structural inhibitors recommending a common interface with Tau for eLife consideration. Your article has been reviewed by three peer reviewers, and the evaluation has been followed by reviewing editor and Cynthia Wolberger as Senior Editor. The following persons involved in the examination of your referral have agreed to disclose their identity: Sara Linse (#1). Reviewers have discussed comments with each other and the Reviewing Editor has drafted this decision to help you prepare for a revised submission. The authors report on the structure of D23N-Ab (16-26) antiparallel cross-β form, design and optimize peptide-based inhibitors based on its structure, and suggest inhibition of Aβ aggregation, cross-seeding tau by adi aggregation of Aβ, and tau aggregation itself. The work is exciting because it shows that Aβ and tau share a common structural function, which is responsible for both Aβ toxicity and cross-seeding tau, which could directly link early Aβ to the aggregation of late tau aggregation - a big question of how aggregation is associated with degeneration of Alzheimer's disease. Work is fundamentally important and the revised manuscript may be suitable for eLife, but there are issues that need to be addressed to ensure that the work reaches eLife's reliability and impact standards. As summarised below, they fall into three categories: (1) The general reliability of assembly reactions in the presence of a polystyrene surface. 2) Better explain the logic of using antiparallel cross-β structure based on designing inhibitors of Aβ2 fibrils, which have parallel structures. (3) Concerns about the technical aspects of the study and the extent to which the different aspects of the system have been adequately characterised. Important issues to address: 1) Impact of the reaction matrix. Please explain why a beta1-42 aggregation is so slow and specify the surface material of the well with 96. If it is normal polystyrene, the reaction may be dominated by the action of polystyrene and avoided in most current studies because it either catalyzes or slows down aggregation depending on the peptide concentration and surface area, and even makes the reaction concentration independent, with the polystyrene surface limiting the reaction rate). Basic kinetic measurements should be repeated on non-ding plates. Related issues include: (i) small effect of 10% Aβ1-42 seed (Figure 5 – Figure 1). Is this a polystyrene artifact? (ii) Please specify the vessel in which the aβ or Aβ plus inhibitor was incubated and the surface material used during the aggregation reactions of other proteins. Can we look here for polystyrene catalyzed aggregation? 2) Inhibitor design strategy Please explain earlier in the text to use antiparallel β structure that is the basis for the development of inhibitors. Inhibitors appear to inhibit the formation of Aβ42 fibrils with parallel β structures. Why, if inhibitors were designed to cap the antiparallel structure? [Related work, Wei Qiang recently showed that structural-based inhibitors can direct D23N-Ab (1-40) self-assembly towards either antiparallel or parallel structures (see J. Phys. Chem.B, vol. 121, p. 5544, 2017)] 3) System characterization (i) Concentration tau is investigated in both in vitro and cell model system. In none of these conditions was the tau phosphorylation status determined/discussed. Of course, in vitro conditions used are not phosphorylation tau. Given that tau phosphorylation is a hallmark of tau neurofibrilary tangles, it is very likely that both tau's biophysical properties and interactions are very well combined with its phosphorylation status. Therefore, it is important to assess whether and how the status of tau phosphorylation affects inhibitor activity. (ii) The authors shall determine whether inhibitors affect the formation of oligomer when antibodies against specific oligomeric/fibrillary builds are used. The effect of inhibitors can only be evaluated in the molar relationship of the Aβ inhibitor 1:10. However, ThT data show that inhibitors are very effective in the 1:1 molar ratio (reduction of more than 80% ThT signal amplitude). Only one of the antibodies used (A11-O9) wasgomers. All other antibodies to the probe against fibrillary nodes. These latest antibodies are expected to not work (ThT is negative in the presence of inhibitors). Therefore, the whole argument is based on the fact that the formation of oligomer affects the result of a single antibody, western blot. These results are not quantified and the authors should specify how many times the experiment was carried out. There are commercial dyes that detect oligomera populations of Aβ, which the authors should use to confirm their single observation. iii) The authors will try to determine whether the inhibitors cap fibril will end as predicted by their design or when they loosen fibrils. The test is to add 72 hours after the ripple begins. The analysis is done through negative staining TEM. The result does not indicate a difference between samples treated with a control or inhibitor (Figure 4B). It is then assumed that inhibitors cap or coat fibrils. A better experiment would be to add inhibitors during the exponential phase of fibile formation. In this case, if the hypothesis is true, fibrill elongation should stop and can be analysed by negative stain analysis of the fibile yield/ThT/AFM or fible length distribution. iv) Subpart Inhibitors bind and reduce the toxicity of Aβ aggregates: the authors report that the Kd value of the D1d inhibitor is bound to Aβ fibrils. The toxicity reduction ic50 of Aβ fibrils, the same inhibitor, is approximately 50 times lower. This makes it difficult to rationalize how 50% of activity is acquired in such a small proportion of inhibitor-related whereas reported Kd. v) Subpart Inhibitors reduce tau aggregation and sowing: the effects of mutageneesis are not judged over the tendency of mutated tau to form fibrils. In fact, not all mutants seed the same efficiency. The authors should provide evidence (negative stain TEM, fibril yield) that tau fibrils are still formed to show that the observed effects are due to specific changes in binding epitops and not the overall effect of fibrill formation caused by mutations. (vi) The number of elements of this test must be verified. First, the total load of tau in different tissues may not be equal. This would explain the observed different seed efficiency indicators (Figure 7A) and allow the results to be interpreted in terms of disease progression, which correlates with tau deposition loads. A control of tau immuno-depletion is necessary to support the claim that inhibitors have direct effects with tau and tau-mediated seeds. Author's fee questions 1) Please describe the country where the ThT analyses begin? How was the monomer isolated? 2) How do I compare the crystal structure with the fibril structure of antiparallel D23N-Aβ(1-40) as described in the comparison with the crystal structure D23N-Aβ(1-40)? It may be appropriate to have a brief discussion. The hydrogen bond register appears to be different. 3) Are preformed Aβ42 nodes fibrills or nonfibrill oil oligomers in Figure 4A? The text is unclear on this issue. 4) Discussions show that tau and Aβ fibrils structures are similar, based on the crystal structures of tau peptides and Aβ peptides (Figure 6). These crystal structures are indeed similar, but are fibrils formed in the structures of full-length Aβ and tau also similar? Several fibril structures are now available in solid state NMR and cryoem, so it would be wise to compare these fibril structures directly, because fragments beyond the amyloid nucleus probably play an important role in modulating the final fibril conversion achieved. This makes it very difficult (if not dangerous) to draw conclusions physiological length of aβ, with a beta16-26-D23N body structure described in the body of aβ16-26-D23N. At least it should be managed as a possible major work warning. (5) Is the effect of inhibitors on the sowing of Aβ fibrils by tau aggregation due to the coating or coating of Aβ fibrils, or is it due to a direct inhibition of tau aggregation (as evidenced by the authors)? (6) The document concludes that direct interaction between Aβ-kernel and tau amyloid-aldi regions facilitates cross-seeding. Can the authors be more specific about what this communication is and how it facilitates cross-seeding and how their data supports this idea? Can tau fibrils grow at the ends of Aβ fibrils? Or aβ fibrils on the sides? Or is the non-fibrillator state of Aβ important? Or perhaps a non-parallallal structure that exists only at the end of Aβ fibrils? Or perhaps tau oligomers form the ends or sides of Aβ fibrils, and then tau fibrils nucleate in these tau oligomers? (7) The work does not provide direct evidence that Aβ has a common surface or motive, as was found in tau. This could have been done simply by mutated Aβ, so that the tau was mutated in this study and repeated ab seeding study tau. 8) The findings of this study are based on the development of peptide inhibitors, as evidenced by the authors, the formation of Aβ fibrils, at the same time as toxicity and sowing. However, the concentration of persistent monomers or oligomers is not estimated in the solution: this is expected to increase due to a decrease in fibrillation. Such data would help to understand the mode of action of the inhibitors presented. 9) Why is the crystalline arrangement of the Aβ16-26 peptide described in this work considered fibril? This is not different from previous steric zippers considered in crystalline arrangements, such as those already described by the same group with steric zippers, Class 7. 10) The efficacy of subpart Aβ-aggregation inhibitors designed against Aβ 16-26 D23N: please specify how the IC50 was evaluated. 11) Subpart Reduction of toxicity by proposed inhibitors can be explained by reducing Aβ1-42 aggregation: the use of negative stain TEM to prove the absence of fibrils is prone to overinterpretation. A more quantitative method, such as fibril yield (or soluble species yield) by centrifugation, would reinforce the authors' argument. 12) There is a related issue that there is generally no characterisation in which particles are induced by interaction with the inhibitor. DLS data would help to identify which species (monomers, oligomers, small fibrils) inhibitors are binding. (13) A better use of the Kd value of a D1d inhibitor associated with Aβ fibrils would be to compare it with D1b peptide Kd, which is less active than D1d. better cope with self-aggregation of analytes that the authors claim to interfere with their SPR-based binding tests. (14) Subpart Inhibitors reduce the seeding of tau by aggregated Aβ1-42 – the authors claim that in their experiments fibrils of addi a beta1-42 seed tau add-on fibrils are as effective as tau K18 fibrils. However, the results do not show a clear reduction in Tlag (Figure 5A), which is expected and clearly observed in Aβ1-42 self-sowing (Figure 5-figure supplement 1, panel B) 15) Subpart Inhibitors reduce the seeding tau aggregated Aβ1-42: the authors suggest that fibrills from hIAPP, TDP43 α,-synapses and TTR are morphologically similar. It's a lie. 16) Subpart Inhibitors reduce tau seeding with aggregated Aβ1-42: observed inhibition of Aβ1-42 fibril seed tau aggregation appears to be dose dependent, except inhibitor D1b. More test points should be provided when responding to inhibitors (Figure 5D). 17) Subpart Inhibitors reduce tau aggregation and sowing: control-LC peptide (L-amino acid version of D1 peptide) increases aggregation in vitro (reduced Tlag In ThT) and cellular analyses (increase in the number of seminal aggregates in tau-K18 biosensor cells). Can the authors comment on how peptide stereochemistry affects induction/inhibition of aggregation? 18) Discussion section four: this work does not characterize the path of aggregation Aβ and tau. It is therefore not appropriate to assume that both molecules have a common aggregation pathway based on susceptibility to the peptide inhibitor. The authors report on the structure of D23N-Ab (16-26) antiparallel cross-β form, design and optimize peptide-based inhibitors based on its structure, and show inhibition of Aβ aggregation, cross-seeding tau aggregation of Aβ, and tau aggregation itself. The work is exciting because it shows that Aβ and tau share a common structural function, which is responsible for both Aβ toxicity and cross-seeding tau, which could directly link early Aβ to the aggregation of late tau aggregation - a big question of how aggregation is associated with degeneration of Alzheimer's disease. Work is fundamentally important and the revised manuscript may be suitable for eLife, but there are issues that need to be addressed to ensure that the work reaches eLife's reliability and impact standards. As summarised below, they fall into three categories: (1) The general reliability of assembly reactions in the presence of a polystyrene surface. 2) Better explain the logic of using antiparallel cross-β structure based on designing inhibitors of Aβ2 fibrils, which have parallel structures. (3) Concerns about the technical aspects of the study and the extent to which the different aspects of the system have been adequately characterised. Important issues to address: 1) Impact of the reaction matrix. Please explain Aβ1-42 aggregation is both slow and refine the surface material 96 well. If it is normal polystyrene, the reaction may be dominated by the effect of polystyrene and that it affects inhibitors (in most current studies, polystyrene is avoided because it catalyzes or slows down aggregation depending on the concentration of the peptide to the area ratio and even makes the reaction concentration independent, since the polystyrene surface limits the reaction rate). Basic kinetic measurements should be repeated on non-ding plates. Related issues include: (i) small effect of 10% Aβ1-42 seed (Figure 5 – Figure 1). Is this a polystyrene artifact? (ii) Please specify the vessel in which the aβ or Aβ plus inhibitor was incubated and the surface material used during the aggregation reactions of other proteins. Can we look here for polystyrene catalyzed aggregation? Thank you reviewers for alerting us to possible interactions between polystyrene and Aβ. Our initial kinetic measurements were performed on polystyrene plates and are part of the improved materials and methods. As suggested, to ensure that the effect of our inhibitors on Aβ is not affected by the plate material, we repeated the experiments as shown in Figure 3A and Figure 5 – Figure 1. We found that lag time decreased ~ 8 hours on polypropylene plates for about 11.5 hours on polystyrene plates. The inhibition results were similar to those for polypropylene wafers as shown in Figure 3 – Figure 1A. Since inhibition was consistent regardless of the type of plate, we did not repeat the aggregation measurements of other proteins (tau, hIAPP, α-synuklein). All the additional tests requested by the reviewers were carried out on polypropylene plates. We are not too worried about the long time in our analyses. We have found that the waiting times for Aβ aggregation are quite different based on the cleaning method, as well as the methodology of the analysis, since the time-point readings interfere with the plate and increase the rate of aggregation. Changing waits from minutes to days at concentrations comparable to those used in our tests have been reported in the Aβ42 literature. Our recombinant Aβ product provides a reproducible cerene waiting period through preparations (see Krotee et al., 2017). We don't remove salts from hPLC purification, like TFA, so adding them to our source material can affect waiting times compared to the faster aggregation rates of SEC insulated monomers where these salts have been removed. 2) Inhibitor design strategy Please explain earlier in the text to use antiparallel β structure that is the basis for the development of inhibitors. Inhibitors appear to inhibit the formation of Aβ42 fibrils with parallel β structures. Why, when inhibitors were designed to limit the antiparallel structure? [Related work, Wei Qiang recently showed that structural-based inhibitors can direct D23N-Ab(1-40) self-assembly towards either antiparallel or parallel structures (see J. Phys. Chem.B, vol. 121, p. 5544, 2017)] We have changed the text in the Results section to further clarify the rationality of our inhibitor design. We have edited the text for the results (sub-division Aβ16-26 D23N atomic structure, determined by MicroED in paragraph two) to add a 1-42 structure to the cryoEM (5OQV) to better explain how inhibition of Aβ42 fibrils can occur when targetingAβ 16-26. Figure 1 adds a structural overlay of Aβ16-26 and Aβ42 fibrils — Figure 2. Although we used an antiparallel structure to shape inhibitors, our goal was to suppress the common structural motif, which occurs in different larger nodes, both antiparallel and parallel. (3) System characterisation (i) Tau aggregation is investigated both in vitro and in the cell model system. In none of these conditions was the tau phosphorylation status determined/discussed. Of course, in vitro conditions used are not phosphorylation tau. Given that tau phosphorylation is a hallmark of tau neurofibrilary tangles, it is very likely that both tau's biophysical properties and interactions are very well combined with its phosphorylation status. Therefore, it is important to assess whether and how the status of tau phosphorylation affects inhibitor activity. It is true that we do not explicitly determine the status of tau phosphorylation, but we are doing everything we can to consider it in the most appropriate possible context by testing the effects of D1b on the human brain derived from tau fibrils in biosensor cells, which are an established model of tau aggregation and create an environment that promotes tau phosphorylation. We argue that the explicit characterization of various possible post-translation changes from the various possible tissues of tau is out of the scope of our manuscript, as such an analysis would require strict testing of the tissues of many other tau donors that are specific to various post-translational changes and/or mass spectrometry. In addition, such an analysis would be speculative, since it has not even been established whether or how the changes following the translation alter the biophysical characteristics and interactions of tau fibrils and whether the changes following tau translation are even fully known or if their frequency has been observed. Most importantly, most ad-related phosphorylation sites have so far been identified outside the K18 area. In the K18 region, phosphorylation of amino acids 258,262, 289 and 356 AD derived tau (Martin, L., Latypova, X., and Terro, F. (2011) for tau protein translational changes: treatment of Alzheimer's disease. Neurochemistry International. 58, 458–471; Duka, V., Lee, J. H., Credle, J., Wills, J., Oaks, A., Smolinsky, C., Shah, K., Mash, D.C., Masliah, E., and Sidhu, A. (2013) Tau hyperphosphorylation and Tau Kinases activation areas for syintesopathy and Alzheimer's disease. One. 8, 1-11) none of which consist of the sequence we have identified to bind inhibitors. In addition, phosphate groups or other ptms are not visible in the atomic structures near tau fibrils, which were resolved in resolutions where the density of such changes can be recognized. (Kenner, L. R., Anand, A. A., Nguyen, H.C., Myasnikov, A. G., Klose, C. J., McGeever, L. A., Tsai, J.C., Miller-Vedam, L. E., Walter, P., and Frost, A. (2019) eIF2B-catalysed nukled stress exchange and phosforegulation integrated. Research. 364, 491 LP – 495). We recommend that while hyperphosphorylation may play a role in tau aggregation (monomer combined), it likely does not play an important structural role in stabilizing the fibril core, and that the binding D1b inhibitor does not rely directly on any given PTM. Therefore, we consider it best to limit our analysis to immunopathologically confirmed cases of tau pathology and to avoid speculation about how post-translation modifications may affect the properties of sowing and inhibition. We will include in our discussion a statement that draws attention to the that various co-factors and/or translational modifications, such as tau phosphorylation, may affect the ability of Aβ to reduce the effectiveness of seed tau and D1b in tau sowing, as referenced in our response to the following question raised in section #4. ii) The authors shall endeavour to determine whether the inhibitors affect the formation of oligomer when using antibodies against specific oligomeric/fiarbrillation. The effect of inhibitors can only be evaluated in the molar relationship of the Aβ inhibitor 1:10. However, ThT data show that inhibitors are very effective in the 1:1 molar ratio (reduction of more than 80% ThT signal amplitude). Only one of the antibodies used (A11-O9) wasgomers. All other antibodies to the probe against fibrillary nodes. These latest antibodies are expected to not work (ThT is negative in the presence of inhibitors). Therefore, the whole argument is based on the fact that the formation of oligomer affects the result of a single antibody, western blot. These results are not quantified and the authors should specify how many times the experiment was carried out. There are commercial dyes that detect oligomera populations of Aβ, which the authors should use to confirm their single observation. We thank the reviewers for this observation and agree that the decrease in oligomer formation has not been sufficiently characterized. We have repeated our dot blot experiment and quantified the A11 (polyclonal) results associated with Aβ samples that are incubated figure 3 — Annex 2 to the figure. We have also included a line in the text (Subsection Reduction of toxicity with the proposed inhibitors can be explained by reducing Aβ1-42 aggregation in the second paragraph) stating that we have not identified which clear oligomerical nodules have been reduced by the addition of our inhibitors. We tried to analyze the formation of oligomer using a color bis-ANS that detects hydrophobicity and is commonly used to monitor the formation of oligomer. Other oligomer-specific dyes such as BD-oligo and other modified BODIPY molecules are not yet commercially available. We found that bis-ANS produced a very strong signal for our inhibitors alone, perhaps due to their hydrophobic nature and self-connection, as well as their limited solubility, which requires the preparation of the DMSO. Therefore, this dye could not be used to monitor the formation of Aβ oligomer by adding inhibitors. iii) The authors will try to determine whether the inhibitors cap fibril will end as predicted by their design or when they loosen fibrils. The experiment is to add inhibitors 72 hours after the ripple begins. The analysis is done through negative staining TEM. The result does not indicate a difference between samples treated with a control or inhibitor (Figure 4B). It is then assumed that inhibitors cap or coat fibrils. A better experiment would be to add inhibitors during the exponential phase of fibile formation. In this case, if the hypothesis is true, fibrill elongation should stop and can be analysed by negative stain analysis of the fibile yield/ThT/AFM or fible length distribution. We thank the reviewers for this proposal. The primary objective of the test in Figure 4B was to demonstrate that fibril structures are not dissolved as this may be one of the mechanisms for toxicity and suppression of sowing. We have suggested that the addition of inhibitors at 1:1 will completely stop fibile growth and 10 Aβ: 1 inhibitor may slow the growth of fibriles, monitored by ThT, and added it to Figure 4 – Figure Supplement 1B. We are careful not to overinterpret the outcome of this test, as the inhibitor may be a free monomer or small assembly separation from the addition to fibrils, not just fibrils already present and has noted it in the text (subsection Inhibitors bind and reduce toxicity to Aβ aggregates paragraph two). iv) Subpart Inhibitors bind and reduce the toxicity of Aβ aggregates: the authors report that the Kd value of the D1d inhibitor is bound to Aβ fibrils. The toxicity reduction ic50 of Aβ fibrils, the same inhibitor, is approximately 50 times lower. This makes it difficult to rationalize how 50% of activity is acquired in such a small portion of inhibitor-related whereas reported Kd. We do not report IC50, which is about 1µM when inhibitors are added to the monomer, which prevents fibrillation. The Kd we report is the binding of the inhibitor D1d to fibrillar Aβ. A better experiment to compare our reported Kd is our experiment with fibrillary Aβ seeding tau biosensor cells (Figure 5C) or Aβ-aggregates treated with an N2a cell inhibitor. We report IC50s in both processes to be at least ~ 5µM, or ~ 10 times lower than our reported Kd. We also see the variability of D1d efficacy in pre-aggregated structures, with it better oligomerical toxicity inhibitor, rather than fibrilse sowing, a process for which our experimental Kd is more applicable. This is not a rare trend: peptide inhibitors are much better at avoiding the aggregation of monomer than reducing the toxicity of already formed aggregates. (v) Subpart Inhibitors reduce tau aggregation and sowing: the effect of mutagenesis is not judged by the tendency of mutated tau fibrils. In fact, not all mutants seed the same efficiency. The authors should provide evidence (negative stain TEM, fibril yield) that tau fibrils are still formed to show that the observed effects are due to specific changes in binding epitops and not the overall effect of fibrill formation caused by mutations. We agree with the reviewers that we have not provided sufficient evidence of the fibrillation of our mutants. To provide evidence, we add our modified manuscript tht and EM mutated tau characterisation in Figure 6 – Figure 2. Mutants do not cause differences in maximum ThT signal, which is not correlated with sowing efficiency. This may be due to tht altered binding of various fibrill structures formed, rather than differences in fibrill load. However, these data confirm that tau fibrils are still formed by each mutant. (vi) The number of elements of this test must be verified. First, the total load of tau in different tissues may not be equal. This would explain the observed different seed efficiency indicators (Figure 7A) and allow the results to be interpreted in terms of disease progression, which correlates with tau deposition loads. A control of tau immuno-depletion is necessary to support the claim that inhibitors have direct effects with tau and tau-mediated seeds. We agree the tau total load probably is not equal to different tissues, and this is probably the reason for the different seed effectiveness that is observed in different tissue types; we have noted this in the amended text (subsection D1b, the engineered inhibitor D1b, is aimed at disease-related body building in the second paragraph). However, our idea is not that D1b works differently in different stages of disease progression, but simply that D1b reduces tau seeding tissue from each of the different regions of the samples, and could be useful in treating patients at different stages of the disease. We simply stress that in this case, this sowning force corresponds to the expected pattern based on Braak's staging. The hippocampus, which is affected before neocortic areas, including forehead and occipital more aggregated tau. We are monitoring stronger sowing from the hippo section, and this may explain the relative reduced partial efficacy of D1b. We have included seeding data in terms of controlling the non-patient patient's brain, as well as the immune system of the depleted PSP brain in Figure 7A to confirm that the misunderstood tatau from tissue mediation. Author's fee questions 1) Please describe the country where the ThT analyses begin? How was the monomer isolated? ThT aβ was prepared by resuspending lyophilised Aβ HPLC by cleaning and filtering nh_4OH as described in the Materials and Methods section. We didn't isolate the monomer by the SEC prior to tht analyses. 2) How do I compare the crystal structure with the fibril structure of antiparallel D23N-Aβ(1-40) as described in the comparison with the crystal structure D23N-Aβ(1-40)? It may be appropriate to have a brief discussion. The hydrogen bond register appears to be different. If both D23N-Aβ(16-26) and D23N-Aβ(1-40) fibril have parallel structures, the former stacks with β sheets are out of the register, the latter is out of the register, which we have now described in the text (atomic structure Aβ16-26 D23N, to be determined by MicroED). So yes, the hydrogen bond register is different. It is this registration difference that makes the D23N-Aβ (16-26) structure have similarities between oligomers, not just fibrils. 3) Are preformed Aβ42 nodes fibrills or nonfibrill oil oligomers in Figure 4A? The text is unclear on this issue. We have added a modified manuscript point bblot (A11, OC, 6E10) to show the types used in Figure 4A in Figure 4A in Figure 4A in Figure 4 – Figure 1. Preformed aggregates are mainly non-fibrillar oligomers, but some fibrillary aggregates are available. 4) Discussions show that tau and Aβ fibrils structures are similar, based on the crystal structures of tau peptides and Aβ peptides (Figure 6). These crystal structures are indeed similar, but are fibrils formed in the structures of full-length Aβ and tau also similar? Several fibril structures are now available in solid state NMR and cryoem, so it would be wise to compare these fibril structures directly, because fragments beyond the amyloid nucleus probably play an important role in modulating the final fibril conversion achieved. This makes it very difficult (if not dangerous) to draw conclusions about the behavior effects of Aβ physiological length of the body building observed in this work Aβ16-26-D23N. At least it should be managed as a possible major work warning. We agree that smaller peptide structures do not always reflect full-length fibrils structures. Although the inhibitors were designed for the Aβ16-26-D23N segment, their efficacy was nevertheless characterised by Aβ 1-42. We have included in the review a comparison of the β16-26-D23N segment with the full length structure determined by the cryoem, showing the similarity to the region used atomic structure in Aβ16-26 D23N atomic structure, determined by a microed system. We have changed the debate (paragraph 4) to make it clear that the overall structure of Aβ and tau full-length fibrils is not similar, but rather that they contain similar surfaces. We have added a model Aβ 1-42 and tau [figure 6-figure supplement 2], where we highlight an interface that could facilitate cross-seeding and be targeted by our inhibitor. We have also noted (discussion section five) that it is possible that D1b may be effective only for a few subtypes of aggregated tau, and that there may be other fibril polymorphors with various structural conformations that may not be sensitive to D1b inhibition. In addition, it is not known how interactions and post-translational agents such as phosphorylation can affect Tau's sowing by the effectiveness of the Aβ or D1b inhibitor. Thus, cross-seeding of Aβ may be one of the many possible structural stimulus of tau aggregation. (5) Is the effect of inhibitors on the sowing of Aβ fibrils by tau aggregation due to the coating or coating of Aβ fibrils, or is it due to a direct inhibition of tau aggregation (as evidenced by the authors)? We cannot rule out that an over-inhibitor can interact with tau monomer, as we can see in the inhibition of the in vitro-induced tau monomer aggregation of heparin in all our inhibitor designs. However, we see a difference in seed inhibition of D1, D1b and D1d when adding fibrils Aβ or tau. Although all inhibitors have similar effect on tau monomer aggregation, D1b is much more effective than other fibril-induced seed inhibitors. In addition, inhibitors D1 and D1d Tau add Aβ-serum at 20 µM, while Tau induced sowing does not decrease at this concentration, suggesting that this is due to interaction with direct inhibition of Aβ fibrils and tau aggregation. (6) The document concludes that direct interaction between Aβ-kernel and tau amyloid-aldi regions facilitates cross-seeding. Can the authors be more specific about what this communication is and how it facilitates cross-seeding and how their data supports this idea? Can tau fibrils grow at the ends of Aβ fibrils? Or aβ fibrils on the sides? Or is the non-fibrillator state of Aβ important? Or perhaps a non-parallallal structure that exists only at the end of Aβ fibrils? Or perhaps tau oligomers form the ends or sides of Aβ fibrils, and then tau fibrils nucleate in these tau oligomers? We have not concluded the exact mechanism of cross-seeding and cannot conclusively claim the interaction that facilitates cross-seeds. Based on the results of our mutagenesis tests, we have included a model of how sowing of aβ fibrils from the sides can take place in Figure 6 – Figure 3.7) The work does not provide direct evidence that Aβ has a common surface or motif, as was found in tau. This could have been simply mutated Aβ, so that tau was mutated in this study and repeating Ab seed study tau. We thank the reviewers for this proposal. We agree that we did not provide enough experimental evidence to provide a common surface for both Aβ and tau. We have included k18 biosensor sowing data and analysis of the text for the two Aβ mutants, Aβ L15R/F17R and K16A/V18A/E22A, starting in subpart Inhibitors to reduce tau sowing in the aggregated Aβ1-42 and Figure 5 – Figure 1. The residue F20 was not altered as it has been shown that both the buried and the surface are accessible in full-length structures. We found that fibrils l15R/F17R seed tau, while fibrils K16A/V18A/E22A is not. In addition, the addition of D1b reduces the sowing of L15R/F17R fibrils. Together, we interpret this as a sign that residues 16/18/22 are important for seeding and that these residues are blocked by D1b, We have also included Segment Ab16-26D23N in our in vitro seeding experiment (Figure 5A) tau K18+, and found that it may be sown, but less effective than K18 or Aβ42 fibril. 8) The findings of this study are based on the development of peptide inhibitors, as evidenced by the authors, the formation of Aβ fibrils, at the same time as toxicity and sowing. However, the concentration of persistent monomers or oligomers is not estimated in the solution: this is expected to increase due to a decrease in fibrillation. Such data would help to understand the mode of action of the inhibitors presented. We agree that the assessment of species could help to understand the way the inhibitors presented work. When a monomer is treated with an inhibitor, we see a reduction in the types detected by A11 and toxicity from the sample, which means the formation of oligomer. We have also included a series of (Reducing the toxicity of proposed inhibitors can be explained by a reduction in Aβ1-42 aggregation), noting that we have not determined what reducing the number of oligomerals reduces by adding our inhibitors. 9) Why is the crystalline arrangement of the Aβ16-26 peptide described in this work considered fibril? This is no different from previous steric zippers, which are considered crystalline arrangements, such as those already described by the same group with steric zippers, Class 7. We changed the text to call it a crystal, a fibril-like arrangement. Although crystalline, these structures are actually fibrils for all criteria, except that they don't have a twist. We and others celebrate these structures with amyloid-like fibrils. They form elongated structures that can grow to contain infinite copies of the monomer. 10) Subsection Aβ-aggregation inhibitor efficacy designed against Aβ 16-26 D23N: please specify how IC50 was evaluated. We have changed the figure legend and materials and methods sections to determine how the IC50 estimate was calculated. 11) Subpart Toxicity reduction proposed can be explained by the reduction of Aβ1-42 aggregation: the use of negative stains to prove the absence of fibrils is prone to overinterpretation. A more quantitative method, such as fibril yield (or soluble species yield) by centrifugation, would reinforce the authors' argument. We thank reviewers for this point and agree that a negative stain on TEM can be overinterpreted to determine the existence or absence of fibrils. However, we use this technique as another method to confirm our ThT results indicate the presence or lack of fibrill formation. Since this test is already a second check, we do not think that our result needs to be further confirmed. 12) There is a related issue that there is generally no characterisation in which particles are induced by interaction with the inhibitor. DLS data would help to identify which species (monomers, oligomers, small fibrils) inhibitors are binding. From our cell and biochemical studies, inhibitors appear to select and may be binding on many forms of Aβ. The limited solubility and self-association of inhibitors has made it characterize what different Aβ particles it binds to complex. We have done our best to characterize the effects of inhibitors on different species (monomer, oligomer, fibril), despite the fact that we do not infer specific work that they bind to. 13) A better use of the Kd value of a D1d inhibitor associated with Aβ fibrils would compare it to D1b peptide Kd, which is less active than D1d. There are also other experimental methods, such as microscale thermoes, which are reported to better cope with self-aggregation analytes that the authors claim to interfere with their S-based pro-PR binding tests. Thank you to the authors for this comment. We agree that the comparison inhibitor D1b would be informative, D1b would not dissolve enough in this experiment. We tried to measure binding itc, but solubility and self-compatibility inhibitors continue to interfere with our tests. We are working to add solubility labels to our inhibitors, which may contribute to some measurement difficulties. (14) Subpart Inhibitors reduce the seeding of tau by aggregated Aβ1-42 – the authors claim that in their experiments fibrils of addi a beta1-42 seed tau add-on fibrils are as effective as tau K18 fibrils. However, the results do not show a clear decrease in Tlag (Figure 5A), which is expected and clearly observed in Aβ1-42 self-sowing (Figure 5-Figure Supplement 1, Panel B) Thanks to reviewers for this observation, and agree that the results of sowing the entire length of the tau40 were inconclusive. We have replaced the current experiment with seeding with k18+fibrils in Figure 5A. This experiment in the modified manuscript does not require the addition of heparin, which may affect the seeding of fibrils added by the tau monomer. We see a clear reduction in waiting times for sowing K18, Aβ42 and Aβ16-26D23N. Our original 5A has now been added to figure 5-figure supplement 1B, and we have included t1/2 calculations in the drawing of the legend, which shows the small seeding effect of lag time tau40 aggregation. 15) Subpart Inhibitors reduce the seeding of tau by aggregated Aβ1-42: the authors suggest that fibrills from hIAPP, TDP43, α-synukleine and TTR are morphologically similar. It's a lie. Thank you for this point, we have changed the text. 16) Subpart Inhibitors reduce tau seeding with aggregated Aβ1-42: observed inhibition of Aβ1-42 fibril seed tau aggregation appears to be dose dependent, except inhibitor D1b. More test points should be provided when responding to inhibitors (Figure 5D). We agree that more data points could be used to determine dosage addiction and IC50s of less effective inhibitors. However, we do not think that adding these additional data points would change our conclusion that D1b is more effective at other inhibitors. 17) Subpart Inhibitors reduce tau aggregation and sowing: control-LC peptide (L-amino acid version of D1 peptide) increases aggregation in vitro (reduced Tlag In ThT) and cellular analyses (increase in the number of seminal aggregates in tau-K18 biosensor cells). Can the authors comment on how peptide stereochemistry affects induction/inhibition of aggregation? It

may be that the demarcation of D-peptide is out of the register, translated into a bond distance perpendicular to 1/2 of the fibril axis in order to maximize the H-link to the amide spine. This translation causes steric overlapping side circuits and incoming β leaves, which are designed as a mechanism of inhibition that is used in the D-peptide. Since H-gluing is satisfied with stacking of the registry, sterici is not expected to overlap between L peptide R groups and incoming β the peptide. Therefore, it should not be discouraged. In fact, we see a certain level of increased aggregation in A.D., as the reviewer notes. It may be that the produced interaction of R groups in the LC native Aβ jada happens to be more hospitable to the native Aβ chain, than homomeric stacking interactions that are common in uninhibited fibril. 18) Discussion section four: this work does not characterize the path of aggregation Aβ and tau. It is therefore not appropriate to assume that both molecules have a common aggregation pathway based on susceptibility to the peptide inhibitor. We agree with the reviewers that we did not show a description of the aβ and tau aggregation paths and have removed it from the text. Sarah L Griner Paul Seidler Jeannette Bowler Kevin Murray Tianxiao Peter Yang Shruti Sahay Michael R Sawaya Duilio Cascio Jose Rodriguez David S Eisenberg Sarah L Griner Paul Seidler Jeannette Bowler Kevin A Murray Tianxiao Peter Yang Shruti Sahay Michael R Sawaya Dui Cascio Jose Rodriguez Tamir Gonen S Eisenberg Stephan Philipp Justyna Sosna Charles G Glabe Sarah L Griner Paul Seidler Jeannler Bowler Kevin A Murray Tianxiao Peter Yang Shruti Sahay Michael R Sawaya Duilio Cascio David S Eisenberg Donors had no role in the design, data collection and interpretation of the study or the decision to submit the work for publication. Thank you M Diamond for gifting the monoclonal biosensor HEK293 cell-line, which expressed tau-K18 (P301S) EYFP in our inhibitor analysis. Thank you Dr. Vinters and Christopher K Williams for supplying patient tissues and immunohistologic tissues. We thank Dan Anderson for his overall support in the lab. Thank you Lorena Saelices for providing TTR fibers and Qin Cao for providing TDP-43 fibers. We thank Lin Jiang for the conversation about Aβ toxicity. Thank you ucla-DOE X-ray crystallography core technology center; Janelia Research Campus visitors program and Ivo Atanasov and the Electron Imaging Center for NanoMachines (EICN) california NanoSystems Institute (CNSI) at UCLA use their electron microscopes. We thank Johan Hattne for our help processing microed data. The UCLA-DOE X-ray Crystallization Core Technology Center is supported in part by the Department of Energy grant DE-FC0302ER63421. Gonen's lab is funded by the Howard Hughes Institute of Medicine. Cynthia Wolberger, Johns Hopkins University School of Medicine, Wesley I Sundquist, University of Utah School of Medicine, United States Sara Linse, Lund University, The article quoted the number generated by polling from the most different sources: Scopus, Crossref, PubMed Central. Central.